ELSEVIER

Fusion Engineering and Design 42 (1998) 289–297

Fusion Engineering and Design

Nuclear heating measurements for SS-316, copper, graphite, tungsten, chromium, beryllium in a copper centered assembly bombarded with 14 MeV neutrons and analysis

Y. Ikeda [a,*], F. Maekawa [a], M. Wada [a], Y. Kasugai [a], C. Konno [a], Y. Uno [a], A. Kumar [b], M.Z. Youssef [b], M.A. Abdou [b]

[a] *Japan Atomic Energy Research Institute, Tokai-mura, Ibaraki-ken 319-11, Japan*
[b] *University of California at Los Angeles (UCLA), Los Angeles, CA 90095-159710, USA*

Abstract

Under ITER/EDA R&D Task T-218, an experiment on nuclear heating was conducted at the Fusion Neutronics Source Facility (FNS) in JAERI in order to provide experimental data of nuclear heating for structural materials and to validate the data and methods relevant to ITER design calculations. Probe materials, SS-316, Cu, W, Zr, Be, Cr and graphite were tested in a copper centered experimental assembly bombarded with 14 MeV neutrons. A calorimetric method and TLDs were employed for total heating and γ-heating measurements, respectively. The measurements were carried out along a central axis of a copper centered experimental assembly. The total heating rate in the probe material was derived from a temperature rise measured by a thermistor attached to the probe. MCNP4A with JENDL-3.2, JENDL-Fusion File and FENDL-1 libraries were used for experimental analyses. Nuclear heating was derived with the use of KERMA factors based on JENDL-3.2 and FENDL-1. The adequacy of the KERMA data is discussed based on nuclear heating ratios of calculation to experiment (C/E).

1. Introduction

The importance of nuclear heating in structural materials has been recognized from the view point of critical system design in ITER. Requirements for the reduction of design margins are stringently addressed in the design criteria. The uncertainty of the data base relevant to nuclear heating is considered as one of the most crucial problems in the designs, not only for inboard shielding against heating of the superconducting magnet, but also for the plasma facing component configurations. Many data libraries have been compiled and implemented in neutron transport code systems [1–6]. The adequacy of KERMA factors of these data libraries has, however, not been thoroughly tested due to the lack of suitable experimental data.

The present work was carried out under the ITER/EDA R&D Task T-218, focusing on further technical development for the detection of very small signals of temperature rise in structural materials, and on demonstration of the feasibility

* Corresponding author. Fax: +81 29 2825709; e-mail: ikeda@fnshp.tokai.jaeri.go.jp

0920-3796/98/$19.00
PII S0920-3796(97)00187-7

of the technique for precise measurements of nuclear heat deposition in a configuration based on the comprehensive ITER First Wall/Blanket/Shield design for validating the relevant nuclear data. The material investigated was copper which was expected to be a heat sink for the high heat flux protection in the first wall blanket of the current ITER design. As the copper heat sink was close to the plasma D-T neutron source, the direct nuclear heating due to 14 MeV neutrons is the most interesting item to be investigated. For this purpose, a experimental assembly made of copper was constructed and the nuclear heating distribution in the copper assembly was studied. Along with the copper materials, nuclear heatings of other potential structural materials such as Be, graphite, Cr, SS-316, Zr and W were measured by putting each material's probe at the very first location in the copper assembly. The calorimetric measurements of total nuclear heating measurements were complemented by preliminary measurements of gamma-heating component through TLDs, on one hand, and dosimetry activation rates at various locations inside a stainless steel assembly that housed the probes, on the other. In addition, comprehensive analysis of the measured heating rates was carried out to see the adequacy of the available KERMA factor libraries, and the particle transport libraries to predict the measured rates. In this report, the results for experimental analyses based on JENDL-3.2 [7] and a part of FENDL-1 [8] with use of MCNP calculations are mainly given.

2. Experiments

2.1. Neutron source

The D-T neutrons were generated by bombarding a tritiated rotating target with a 20 mA deuteron beam (d^+) accelerated to 350 kV at FNS [9]. The absolute neutron yield was monitored by a ^{232}Th fission chamber which was calibrated by the associated alpha-particle counting method [10]. Nominal neutron yield at the target was $3 \sim 4 \times 10^{12}$ ns^{-1}. The D-T neutron target was located at the center of the target room with dimensions of $5 \times 5 \times 4.5$ m, surrounded by a 2.5 m thick ordinary concrete walls. The neutron irradiation history was recorded with MCS (multi-channel scaling) with a 10 s time bin.

2.2. Experimental assembly

The schematic cross sectional views of the experimental assembly are given in Fig. 1. The central zone of the assembly consisted of copper blocks with a central channel hole of 50 mm in diameter. The cross section of the central zone of copper measured 150×150 mm. In addition to this central region, approximately 100 mm thick of copper region were stacked, followed by a 100 mm polyethylene layer. The assembly was contained in an air tight SS-304 container to insulate the ambient change in room temperature. This configuration minimizes the thermal conduction and convection from the surrounding area. The outer dimension of the container was $600 \times 600 \times 600$ mm. All probe materials of 48 mm in diameter and 48 mm in height to be tested were placed into the center channel. Six probes were aligned with 2.3 mm gaps between each. The assembly was set in front of the D-T neutron target and the distance between the target outer surface and the front surface of the assembly was 14 mm. The axis of the central channel was aligned to the d^+ beam direction in order to keep a good symmetric configuration. The height of the d^+ beam line was 1.8 m from the ground floor.

2.3. Total nuclear heating measurement

The microcalorimeter was employed as the principal technique to measure the total nuclear heating rate in the materials by the neutron and gamma-ray mixed radiation field [11–14]. The microcalorimetric technique is comprised of three components: (1) the material (probe) to be tested; (2) thermal sensors for detecting the temperature rise; and (3) a data acquisition system. Nuclear heating in probe materials of type 316 stainless steel, beryllium, graphite, copper, zirco-

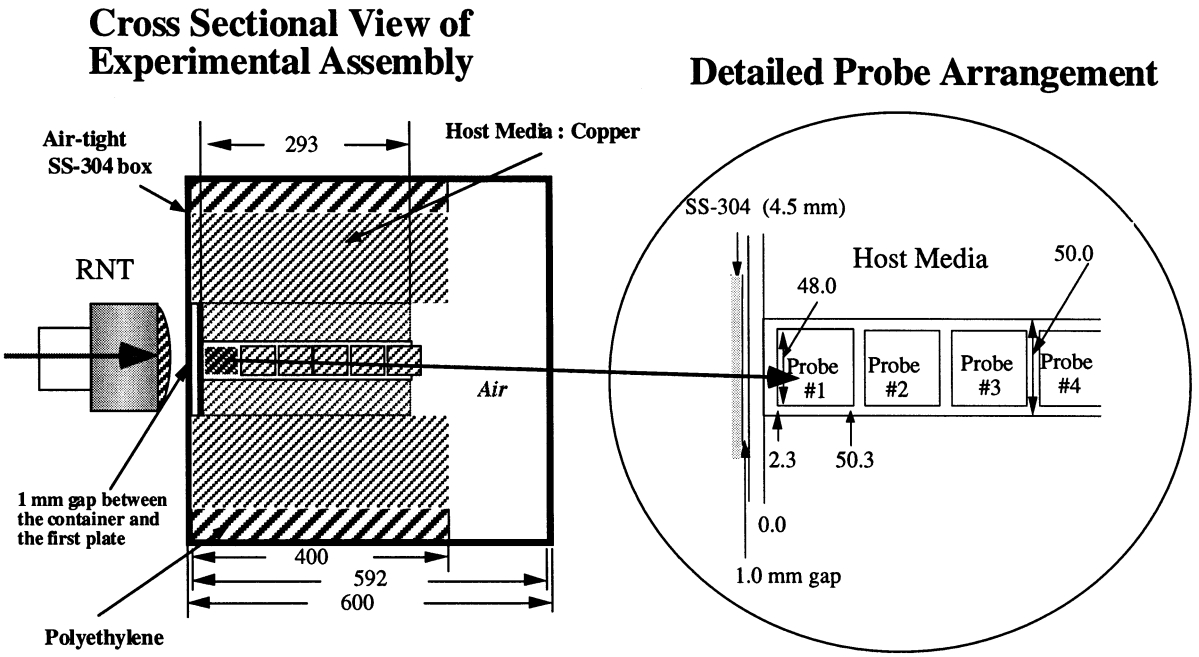

Fig. 1. The copper experimental assembly for the nuclear heating measurement by the calorimetric technique. Dimensions given in the figure are in millimeters.

nium and tungsten were measured. The probe materials were placed inside a cylindrical central channel. Six separate probes of copper were aligned one after another in this channel for the measurement of nuclear heat distribution throughout the assembly. The dimensions of the material configuration in the experimental assembly are given in Fig. 1. To measure nuclear heating of other materials, the first front copper probe of the reference assembly was replaced by a probe of another material, one by one. The distance of the first probe from the neutron source target surface was estimated to be ~ 29 mm. As the thermal sensor, thermistors (TM) with 5 or 10 kΩ at 25°C were used and attached to the front, middle side surface and rear surface of the probe. The probe was supported by a thin piece of carbon paper in order to reduce thermal conduction. The sensors were connected by thin wires with voltmeters (Keithley 182). The coefficient of the sensors for the temperature change were obtained by an off-line calibration procedure. A constant current of 10 μA was applied on 10 kΩ TM.

2.4. Gamma-heating measurement

Thermoluminescent Dosimeter (TLD) has been employed as the γ-ray heating detector. Five different types of TLDs, i.e. BeO ($Z_{\text{eff}} = 7.12$), ^{7}LiF ($Z_{\text{eff}} = 8.24$), MSO (Mg_2SiO_4, $Z_{\text{eff}} = 11.1$), SSO (Sr_2SiO_4, $Z_{\text{eff}} = 32.5$) and BSO (Ba_2SiO_4, $Z_{\text{eff}} = 49.9$), were used to measure γ-ray heating rates of beryllium ($Z = 4$), carbon ($Z = 6$), SS316 ($Z_{\text{eff}} = 26.4$), copper ($Z = 29$), zirconium ($Z = 40$) and tungsten ($Z = 74$). Gamma-ray heating rates of SS316, copper and zirconium could be derived from the interpolation of measured heating rates by TLDs due to the Z-numbers of the materials, 26.4, 29 and 40, being inside the range of the TLD's Z-numbers between 7.12 and 49.9. However, extrapolation or other assumptions were needed for beryllium, carbon and tungsten since no TLDs where Z-numbers were smaller than 7.12 or larger than 49.9 were available. All of the TLDs in powder form were sealed in glass capsules of 2 mm in outer diameter and 12 mm in length. Three kinds of TLDs, i.e. BeO, ^{7}LiF and MSO, were selected for the beryllium and carbon

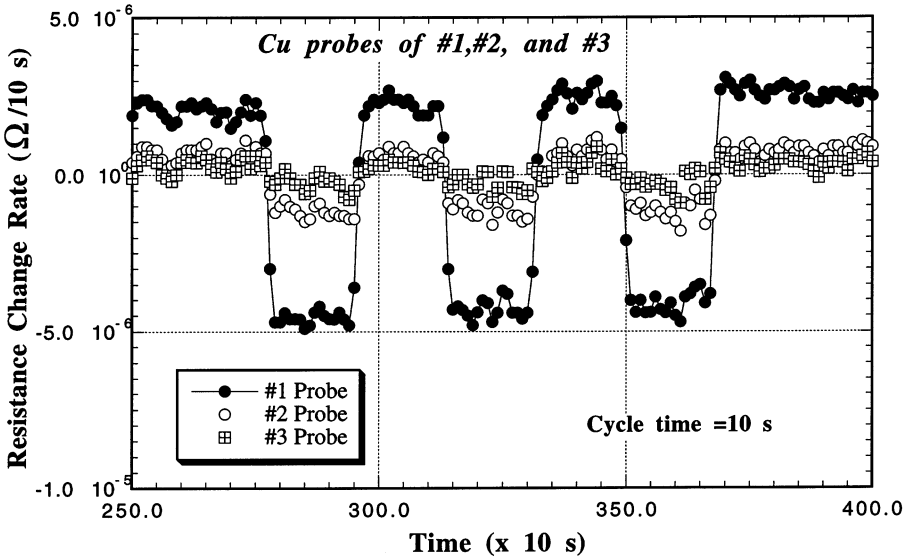

Fig. 2. Derivatives of the temperature rise data on the first copper probes. The rectangular shape drops in the derivatives correspond to the temperature rise due to nuclear heating by D-T neutron irradiations.

measurement, while the other three kinds of TLDs, MSO, SSO and BSO, were used for the SS-316, copper, zirconium and tungsten measurements. Four capsules of TLD were packed in aluminum foil to prevent the TLDs from exposure to light.

3. Measurement

3.1. Measurement of nuclear heating with micro-calorimeter

The calorimeter system was placed very closely to the D-T neutron target, and irradiated with 3 min duration neutron pulses separated by 3 min. A constant current of 10–20 μA was applied to the thermal sensors to detect the signal during the irradiation. The temporal derivative is demonstratively shown in Fig. 2 for very first probes of copper in the reference assembly. There is a TM both at the front and rear of this probe.

The raw resistance change data for a sensor is treated to obtain net resistance change rates. They are then converted to the corresponding heat deposition rate by using specific heat of each material, neutron yield and temperature coefficient of the sensor. The specific heat of each probe material used was taken from available data handbooks. The volume averaged experimental data were derived from the derivatives of the several points at the very end of the irradiation. The temperature rise is assumed to be in equilibrium after 3 min even though the thermal conduction of SS-316 is relatively low in comparison with other metallic materials. The self-heating driven by the joule heat in the resistance of the thermistor sensor gives a constant heating load which contributes to a constant change in temperature. The overall experimental error consists of fluctuation of background in temperature change, specific heat data, and the D-T neutron yield. The errors ranged from 5 to 50%, depending on the signal to noise ratio and conditions of probe in terms of thermal equilibrium.

3.2. Gamma-ray heating rate by TLD

For the copper configuration, positions of TLD packages for the shorter irradiation were 2.0, 52.6, 103.4, 154.0 and 204.7 mm, and those

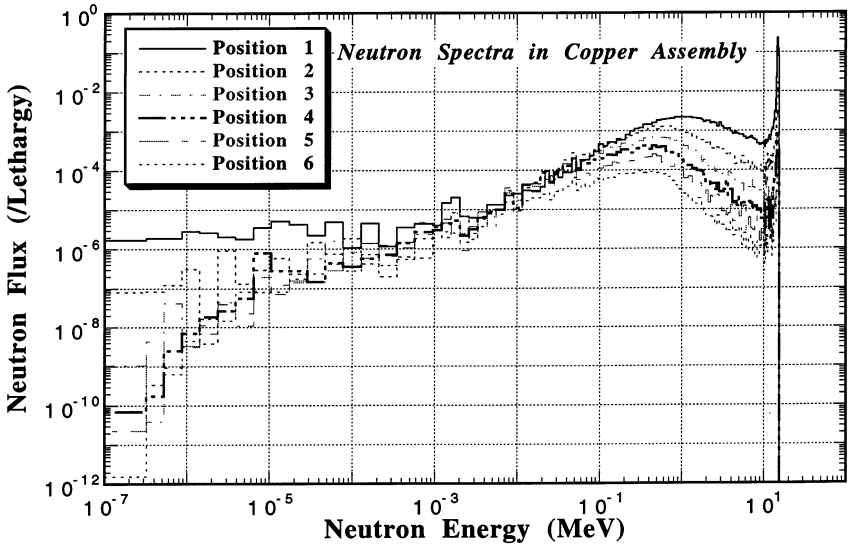

Fig. 3. Neutron spectra at various depths in the copper assembly calculated by MCNP with the FSXLIB-J32 JENDL-3.2 based nuclear library.

for the longer irradiation were 154.0, 204.7, 255.5 and 306.0 mm. One TLD package without an irradiation was kept together in the box. One week after the irradiation, thermoluminescences (TLs) were read out by a TLD reader. The measured TLs were in the unit of equivalent exposure dose of ^{60}Co in air, and they ranged between 1×10^{-4} and 2×10^{-2} C/kg. The range of exposure dose was adequate for the TLDs because a high signal to noise ratio larger than 150 was attained and the linearity of the TLDs were assured as it was better than 3% in the range.

After the subtraction of the neutron contribution, the TL's were converted to gamma-ray heating rates in the unit of Gy/source neutron by considering the differences of mass energy absorption coefficients of air and TLD materials. Error sources of the measured gamma-ray heating rates were as follows: (1) deviations among a group of four TLDs ranged 5–17%; (2) neutron yield was 2%: (3) calibration of the TLD reader was 5%. In the subtraction of neutron response, the following uncertainties were added to the errors according to the law of error propagation: (i) Neutron response function was 30%; and (ii) neutron energy spectra was 10%.

4. Experimental analysis

The 3D code MCNP-4A [15] was used for modeling the rotating target geometry and the probe-vacuum chamber system. The library, FSXLIB-J3.2 [16], was used for neutron interactions and photon production in MCNP calculations in the whole system. Neutron spectra at each probe location are shown in Fig. 3. Also the FENDL-1 library was applied for the MCNP calculation. Heating numbers from FUSION-J3.2 and DLC-99 [17] for neutron and gamma-ray, respectively, were used in the computation of nuclear heating rates for the JENDL calculation. For FENDL calculations, heating numbers based on FENDL-1 were delivered by RSIC. The nuclear heat deposition rate, expressed in Jg^{-1}, is derived and compared with experimental data which were converted from temperature rise to the same energy deposition unit in Jg^{-1}. The D-T neutron target and other important structural components nearby were included in the modeling.

The measured heating rates were compared with the calculated ones. Clearly, the comparison should stand as an indication of the feasibility of these calorimetric experiments themselves. For

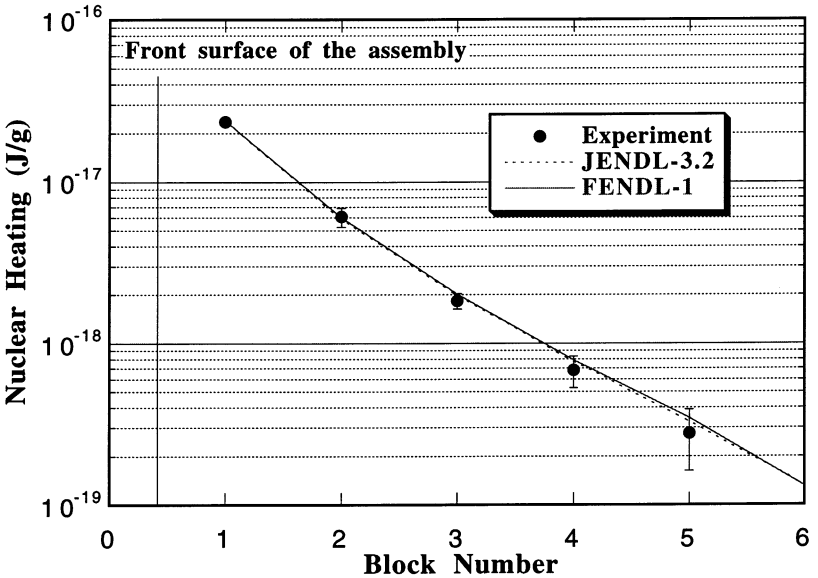

Fig. 4. Measured total nuclear heating distribution along the central axis of the copper assembly. The results of calculations by JENDL and FENDL are shown for comparison.

this purpose, the volume averaged heating rate in the first probe of each of the six experimental assemblies was compared. Before we present the comparison between the calculation (C) and the experiment (E), it is very helpful to understand also the potential sources of discrepancies that can creep into the calculations in the same spirit as was done earlier for the experimental sources of error.

5. Results and discussion

5.1. Total heating

Experimental data were obtained with errors less than 5% for the probes at the first location. Longer cycle time increase the sensitivity for temperature detection at the deeper probes. As a result, experimental data were obtained up to 30 cm in depth. The measured total nuclear heating distribution in the copper assembly is shown in Fig. 4 along with calculations. Both JENDL and FENDL agreed within error with measurements for the heating rate distribution. Ratios of calculation to experiment (C/E) are given in Figs. 5 and 6 for the total heating of the copper assembly and other materials investigated, respectively. The following are the status of the nuclear data for each material:

Cu: Both JENDL and FENDL predictions are identical and agree with the experiments. As there are reasonable agreements for the γ-heating data, it is suggested that both libraries seem adequate for Cu.

C: JENDL overestimates the experiments by 10–15%, while FENDL agrees within the error with the experiments. As it is suggested that JENDL KERMA for carbon is higher than available experimental data in the 14 MeV region, the overestimation in JENDL could be solved after a revision of the KERMA data.

SS: Both calculations agree with the experiment. However, JENDL is higher than FENDL by 10%. It may be due to the difference in the KERMA data.

W: Both JENDL and FENDL overestimate the experiment by 20–30%. As the heating of tungsten was dominated by gamma-heating, these overestimations could be attributed to the overestimation of gamma heating. The secondary gamma production data may need to be examined. Further investigation is necessary.

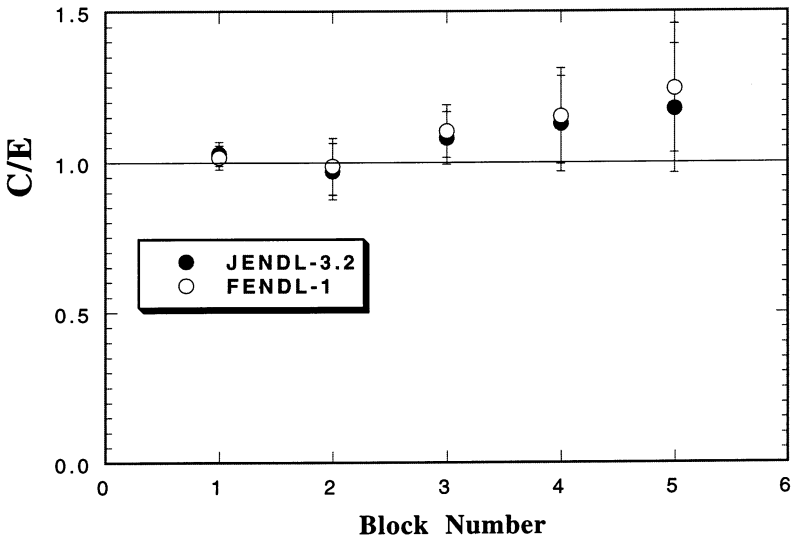

Fig. 5. C/E values for the total nuclear heating of copper probes.

Zr: Although the calculations are overestimated slightly, agreements are in a reasonable range.

Be: As shown in the last experiment with the SS-316 assembly, a large underestimation in JENDL calculations by 25% was observed, whereas FENDL gives better agreement with the experiment. This JENDL underestimation is simply due to the unreasonably low KERMA data at neutron energy above 6 MeV. In conclusion, FENDL seems adequate.

Cr: JENDL and FENDL gives almost identical results, underestimating the experiment by 10%.

5.2. Gamma heating

Fig. 7 shows C/E values for the γ-heating rates. Experimental data were obtained with errors less than 30%. The measured heating rates at the front side are systematically lower than those at the back side. If the contribution from the D-T source is underestimated, this could be explained. However, it is very complicated identifying the source of the systematic discrepancies. The status of the results based on the experimental analysis are as follows:

Cu: With the exception of the first probe, both JENDL and FENDL agree within experimental errors with the experiment.

Be: Both JENDL and FENDL underestimate the experiment by 40–25%.

C: If the data at the backside is taken, both calculations agree within experimental error with the experiment.

Cr: Although there is slight underestimation, JENDL and FENDL both agree with the experiment.

SS: JENDL agrees with the experiment, while FENDL underestimates the measurement by 10%.

Zr: Both JENDL and FENDL agree with the experiment within experimental error.

W: A large overestimation is observed. Even though the experimental error is large, calculations continue to overestimate the experiment. The overestimation is consistent with as overestimation found in the total heating rate measurement to be shown.

As a whole, FENDL tends to give lower values than JENDL. In general, the results are consistent with the results for total heating data.

6. Conclusion

The adequacy of nuclear heating calculations with current nuclear data were studied by experiments under ITER/EDA R&D task T-218. The

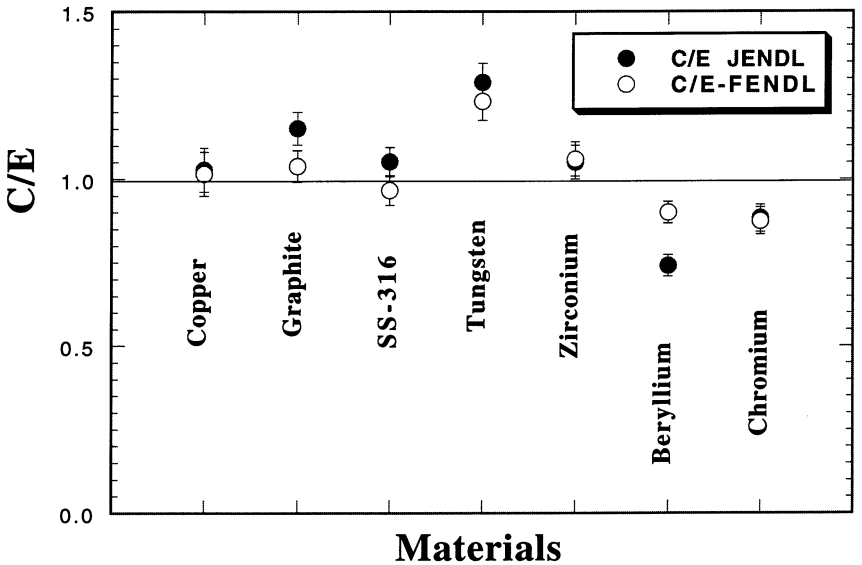

Fig. 6. C/E values for the total nuclear heating of other probe materials at the first location in the copper assembly.

result provided an uncertainty range in the design calculations relevant to the nuclear heating.

Acknowledgements

The authors would like to thank C. Kutsukake, S. Tanaka, Y. Abe, M. Seki for the operation of the FNS accelerator.

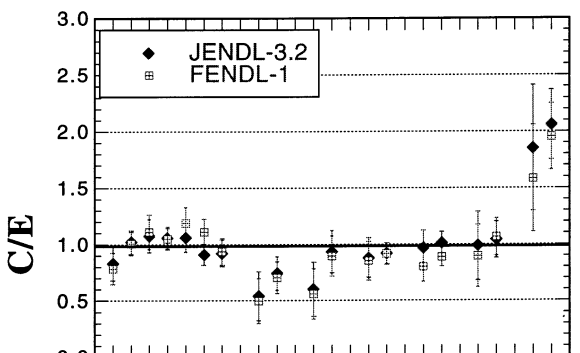

Fig. 7. C/E values for γ-heating.

References

[1] M.A. Abdou, C.W. Maynard, R.Q. Wright, MACK: A Computer Program to Calculate Neutron Energy Release Parameters (Fluence-to-Kerma Factor) and Multigroup Reaction Cross Sections from Nuclear Data in ENDF Format, ORNL-TM-3994 (1973).

[2] M.A. Abdou, C.W. Maynard, Calculation method for nuclear heating—part I: theoretical and computational algorithms, Nucl. Sci. Eng. 56 (1975) 360.

[3] M.A. Abdou, C.W. Maynard, Calculation methods for nuclear heating—part II: applications to fusion reactor blanket and shields, Nucl. Sci. Eng. 56 (1975) 381.

[4] Y. Farawila, Y. Gohar, C.W. Maynard, KAOS/LIB-V: A Library of Nuclear Response Functions Generated by KAOS-V Code from ENDF/B-V and Other Data Files, ANL/FPP/TM-241 (1989)

[5] K. Maki, H. Kawasaki, K. Kosako, Y. Seki, Nuclear Heating Constant KERMA Library, JAERI-M 91-073 (1991).

[6] M. Kawai, et al., Review of the Research and Application of KERMA Factor and DPA Cross Section, JAERI-M 91-043 (1991).

[7] K. Shibata, et al., Japanese Evaluated Nuclear Data Library, Version-3, JAERI-1319 (1990).

[8] S. Ganesan, H. Wienke, FENDL/MC-1.0 Library of Continuous Energy Cross Sections in ACE Format for Neutron-Photon Transport Calculations with the Monte Carlo Neutron and Photon Transport Code System MCNP 4A, IAEA-NDS-169, International Atomic Energy Agency (1995).

[9] T. Nakamura, H. Maekawa, J. Kusano, Y. Oyama, Y. Ikeda, C. Kutsukake, S. Tanaka, Shu. Tanaka, Present Status of the Fusion Neutron Source (FNS), Proc. 4th Symp. on Accelerator Sci. Technol., RIKEN, Saitama, 24–26 November, 1982, pp. 155–156.

[10] H. Maekawa, Y. Ikeda, Y. Oyama, S. Yamaguchi, T. Nakamura, Neutron Yield Monitors for the Fusion Neutronics Source (FNS), JAERI-M 83–219 (1983).

[11] Y. Ikeda, A. Kumar, C. Konno, K. Kosako, Y. Oyama, F. Maekawa, H. Maekawa, M.Z. Youssef, M.A. Abdou, Measurement and analysis of nuclear heat depositions in structural materials induced by D-T neutrons, Fusion Technol. 21 (3) (1992) 2190.

[12] Y. Ikeda, A. Kumar, K. Kosako, C. Konna, Y. Oyama, F. Maekawa, Z. Youssef, M.A. Abdou, H. Maekawa, Integral test of KERMA data for SS-304 stainless steel in the D-T fusion neutron environment, Fusion Eng. Des. 28 (1995) 769.

[13] Y. Ikeda, A. Kumar, C. Konno, K. Kosako, Y. Oyama, F. Maekawa, H. Maekawa, M.Z. Youssef, M.A. Abdou, Direct nuclear heating measurements and analyses for structural materials induced by deuterium-tritium neutrons, Fusion Technol. 28 (1) (1995) 156.

[14] A. Kumar, Y. Ikeda, M.A. Abdou, M.Z. Youssef, C. Konno, K. Kosako, Y. Oyama, T. Nakamura, H. Maekawa, Direct nuclear heating measurements and analyses for plasma-facing materials, Fusion Technol. 28 (1) (1995) 173.

[15] J.F. Breismeister (Ed.), MCNP—A General Monte Carlo Code for Neutron and Photon Transport: Version 3A, report no. LA-7396-M, Rev. 2, September 1988 (along with MCNP3B newsletter dated July 18, 1988), Los Alamos National Laboratory.

[16] K. Kosako, F. Maekawa, Y. Oyama, Y. Uno, H. Maekawa, FSXLIB-J3R2: A Continuous Energy Cross Library for MCNP Based on JENDL-3.2, JAERI-Data/Code 94-020, Japan Atomic Energy Research Institute (1994).

[17] R.W. Roussin, J.R. Knight, J.H. Hubbell, R.J. Howerton, Description of DLC 99/HUGO Package of Photon Interaction Data in ENDF/B-V Format, ORNL/RSIC-6 (ENDF-335) (1983).